An anion exchange membrane electrode assembled photoelectrochemical cell with a visible light responsive photoanode for simultaneously treating wastewater and generating electricity

Hao Feng[a,b,c], Ming Chen[a,b], Rong Chen[a,b]*, Xun Zhu[a,b], Qiang Liao[a,b], Dingding Ye[a,b], Biao Zhang[a,b], Liang An[d], Youxu Yu[a,b], Wei Zhang[a,b]

[a] Key Laboratory of Low-grade Energy Utilization Technologies and Systems (Chongqing University), Ministry of Education, Chongqing 400030, China

[b] Institute of Engineering Thermophysics, Chongqing University, Chongqing 400030, China

[c] MIIT Key Laboratory of Thermal Control of Electronic Equipment, School of Energy and Power Engineering, Nanjing University of Science & Technology, Nanjing 210094, China

[d] Department of Mechanical Engineering, The Hong Kong Polytechnic University, Hung Hom, Kowloon, Hong Kong, China

*Corresponding author. Tel.: 0086-23-65102019; fax: 0086-23-65102474; e-mail: rchen@cqu.edu.cn

Abstract

In this work, an anion exchange membrane electrode assembled photoelectrochemical cell is designed for simultaneously degrading organics and generating electricity. The proposed photoelectrochemical cell is formed by assembling a visible light responsive photoanode and an air-breathing cathode with an anion exchange membrane. Benefited from the intrinsic property of the anion exchange membrane, the hydroxyl transport can be enhanced and the organics crossover can be reduced to improve the performance of the proposed photoelectrochemical cell. Experimental results show that increasing the electrolyte concentration and light intensity yields higher performance because of the more efficient capture and generation of photo-excited holes. Besides, the cell performance can also be enhanced with increasing ethanol concentration in the testing range, demonstrating the lowered ethanol crossover through the anion exchange membrane and mixed potential at the cathode. The obtained results are useful for not only the optimization of the photoelectrochemical cell design but also the promotion of its practical application.

Keywords: Anion exchange membrane; Membrane electrode assembly; Photoelectrochemical cell; Visible light response; Air-breathing cathode

1. Introduction

Water pollution is now a global issue accompanying with rapid development of human society [1-3]. To solve this problem, various technologies for wastewater treatment have been proposed, e.g. the physical adsorption [4], membrane distillation [5], chemical oxidation [6], biodegradation [7]. Actually, there exists a huge amount of energy stored in the wastewater in the form of chemical energy [2, 8, 9]. Although the above technologies can effectively remove the hazardous substances (metal ions, pathogen, organics, etc.), the non-use of chemical energy in the wastewater results in the abundant waste of energy [8, 10, 11]. Moreover, a great deal of energy is consumed during these processes. Hence, a solution to simultaneously recover the energy from the wastewater and degrade the hazardous substances is of great importance for the relief of both the environmental pollution and energy crisis. In recent, the photoelectrochemical cell (PEC) has been deemed to be one of the most competitive candidates for the wastewater treatment due to its intrinsic advantage of not only simultaneous degradation of various organic pollutants and electricity generation, but also the potential usage of the solar energy. Because of these conspicuous features, PECs have attracted wide attractions all over the world [10-13].

Generally, main strategies for the intensification of the PEC performance can be divided into two orientations: (1) the development of highly-efficient photocatalysts [14-16], and (2) the optimization of the PEC design [8]. Currently, the most commonly used photoanode catalyst is TiO_2. However, limited by the wide bandgap, it can only respond

to UV light. To improve the performance of the photoanode and the utilization of solar energy, more effective photoanode catalysts have been developed through various methods like doping, sensitization, etc. [17-19] For example, He et al. [20] proposed a ZnO/TiO_2 nanorod array photocatalyst and demonstrated its promising application in the photodegradation of organic pollutants. Jiang et al. [21] developed the N-doped TiO_2 nanotubes through solvothermal synthesis, the photo-response of the prepared photocatalyst was broadened to visible light and the photocatalytic performance could be significantly intensified. Antoniadou et al. [22] sensitized the TiO_2 by CdS-ZnS for the purpose of the visible-light response. Regarding the PEC design, the conventional constructions typically include the single-compartment [23] and double-compartment [24]. Such batch reactor design usually suffers from poor mass transfer, specially the limited oxygen transport as a result of low solubility of oxygen [25]. To overcome these defects, the membrane electrode assembled photoelectrochemical cell was proposed [8]. Different from the conventional reactor using batch design, the membrane electrode assembly (MEA) design, which has been extensively employed in various proton exchange membrane fuel cells [26], can offer the advantages of the reduced mass transfer resistance and more flexible and compact system.

To date, some works have demonstrated the merits of the combination of the MEA design with the PEC [27, 28]. In these works, the proton exchange membrane was usually used to construct the membrane electrode assembly, as illustrated in Figure 1a. On the other hand, previous works have also demonstrated that the PEC can perform an

excellent performance in an alkaline environment, since a large amount of hydroxyl in the electrolyte can easily combine with the photo-excited holes to form hydroxyl radicals that have strong oxidizability, which could not only directly facilitate the separation of electro-hole pairs but also promote the oxidation rate [10]. However, although the commonly used proton exchange membrane has been demonstrated to be able to transfer the charge carrier of the OH^- ion [29], the transport of hydroxyl mainly relies on the diffusion, which may be restricted because of negative charged functional groups. In this work, hence, an anion exchange membrane, which could enhance the hydroxyl transport and reduce the organics crossover, was used to develop an anion exchange membrane based membrane electrode assembled photoelectrochemical cell (AMEA-PEC) for simultaneous degradation of organics and generation of electricity. Furthermore, considering that the photosensitization by narrow band gap material of CdS is able to broaden the adsorption spectrum to enhance the solar energy utilization and ZnS can be used to passivate CdS to avoid the inherent defect of photo-corrosion [30], CdS-ZnS quantum-dot-sensitized TiO_2 (denoted as CdS-ZnS/TiO_2) was utilized to prepare the photoanode so that the proposed AMEA-PEC could respond to visible light. To facilitate the transport of oxygen and simplify the system of PEC, a cathode with air-breathing mode was employed. The performance of the proposed AMEA-PEC was then evaluated in an alkaline environment.

2. Materials and Methods

2.1 Chemicals and materials

In this work, all the chemicals and materials were used as received. Aeroxide P25 TiO_2 nanoparticles used for the preparation of the TiO_2 colloid were purchased from Acros Organics (Belgium). Acetylacetone and Triton X-100 were obtained from Sigma-Aldrich (USA). Polyethylene, cadmium nitrade, zinc nitrade and sodium sulfide were supplied by Aladdin Industrial Inc (Shanghai, China). Polyethylene grafted polystyrene quaternary ammonium anion exchange membrane (HoAM G1204-05) used in this study was received from Lvhe Technology Co., Ltd (Hangzhou, China). Toray 090 carbon paper, Pt black, Nafion® perfluorinated resin and Nafion® 211 proton exchange membrane were acquired from Hesen Electric Co., Ltd (Shanghai, China). Water used in all experiments was obtained from a ROMB Ultrapure Water System for Laboratory (Chongqing, China).

2.2 Construction of MEA

The MEA consisted of three parts: a photoanode, a cathode and an anion exchange membrane. Before the membrane electrode assembly, the photoanode and cathode were prepared, respectively.

2.2.1 Photoanode preparation

For the photoanode, the preparation procedure can be divided into two steps: the TiO_2 film construction on the carbon paper and the CdS-ZnS quantum-dot-sensitization. In

the first step, the spray-coating method was used for the TiO_2 film preparation. Briefly, the TiO_2 colloid, whose preparation could refer to the previous method [31], was sprayed on the carbon paper with the exposed area of 2.0 cm × 2.0 cm by a spray gun. After the spray coating, the carbon paper with TiO_2 was calcined at 550 ℃ for 2 hours in a tube furnace under the air atmosphere. The obtained TiO_2 loading on the carbon paper was about 3 mg/cm^2. In the second step, the CdS-ZnS quantum-dot sensitization of TiO_2 film was realized by the successive ionic layer adsorption and reaction (SILAR) [32]. Before the sensitization, the precursor solution containing cadmium nitrate and zinc nitrate with the concentration of 75 mM and 25 mM, and the 100 mM Na_2S solution were prepared. Afterwards, the TiO_2 coated carbon paper was first immersed in the precursor solution for 4 min and then put into the Na_2S solution for 5 min for the formation of CdS-ZnS quantum-dots. Completing the above mentioned two processes corresponded to one SILAR cycle. After four SILAR cycles, the obtained carbon paper with coated CdS-ZnS/TiO_2 photocatalyst was dried with nitrogen and heated at 100 ℃ for 10 min. To evaluate the loading of the CdS-ZnS sensitizing agents, the photoanode was weighed before and after the quantum-dot-sensitization by using an analytical balance (BSA224S-CW, Sartorius, Germany), and it was shown that the CdS-ZnS loading was about 0.77 mg/cm^2, which accounted for about 20.5% of the total photocatalysts.

2.2.2 Cathode preparation

In this work, the cathode was also formed through the spray-coating method, in which

the Pt black was deposited on the carbon black coated carbon paper. During the preparation process, the Pt dispersion solution was first prepared by adding 0.1 g Pt black electrocatalyst into the mixed solution containing distilled water (2.5 g), isopropanol (2.5 g) and Nafion® perfluorinated resin (0.5 g). Then, the obtained Pt dispersion solution was sprayed on the carbon black coated carbon paper with the exposed area of 2 cm × 2 cm. Through using the same analytical balance to evaluate the loading of the cathode catalyst, the final Pt loading could be determined to be about 1 mg/cm^2 after the spraying. At last, the prepared cathode was heated at 80 ℃ for 30 minutes.

2.2.3 Assembly and cell fixture

After the preparation of the photoanode and cathode, the membrane electrode assembly was constructed by directly holding the cathode with Pt coated side facing the anion exchange membrane and the photoanode with no catalyst side facing the other side of the anion exchange membrane. Figure 1a schematically shows the exploded view of the AMEA-PEC, which consisted of a photoanode PMMA cover plate, two stainless steel electrical current collectors with the thickness of 1 mm, a MEA and a cathode PMMA cover plate. For the photoanode electrical current collector, the width and the rib size of the serpentine channel fabricated by laser cutting was 1 mm and 1.15 mm, respectively, which provided the transport paths of light and solution. The open ratio of the photoanode electrical current collector was 0.5. For the cathode electrical current collector, four open channels with the width of 3 mm and length of 2 cm were drilled

for the oxygen transport. In the center of the cathode PMMA cover plate, a square hole with the length of 2 cm and width of 2 cm was incised for transport of oxygen. These parts were clamped together by bolts to form the AMEA-PEC.

2.3 Experimental setup

Figure 1b schematically shows the diagram of the experimental system. As shown, a LSP04-1A syringe pump (Longer-Pump, China) was utilized to continuously supply the mixture solution containing the electrolyte of KOH and the model organic pollutant into the cell. The open circuit voltage (OCV), short circuit current density (SCCD) and polarization curves were recorded by a 34972A data acquisition unit (Agilent, USA) and a CT-3008 electronic load (Neware Technology Ltd., China). An adjustable CEL-HXF300 300W Xe lamp (Aulight, China) with AM 1.5G filter was used to simulate the solar illumination to the cell. The light intensity on the photoanode was measured by a FZ-Z visible radiometer.

3. Results and discussion

3.1 Working principle of AMEA-PEC

Figure 2 shows the working principle of the proposed AMEA-PEC. During the working process, the model wastewater is continuously delivered into the photoanode of the cell along the serpentine channel. The oxygen transferred through the carbon paper to the cathode catalyst layer. Upon illumination, the photons through the serpentine are able to photo-excite electron-hole pairs in the photoanode [8, 33].

$$TiO_2 + h\nu \rightarrow TiO_2(h^+ + e^-) \quad (1)$$

Because the photo-generated holes can be easily captured by the OH^- ions and then generate hydroxyl radicals that have strong oxidizability to oxidize the organics [10, 34].

$$h^+ + OH^- \rightarrow \bullet OH \quad (2)$$

$$C_2H_5OH + 12 \bullet OH \rightarrow 2CO_2 + 9H_2O \quad (3)$$

Simultaneously, the generated electrons transport from the photoanode to the cathode via the external load, proceeding the cathodic oxygen reduction reaction [10].

$$2H_2O + O_2 + 4e^- \rightarrow 4OH^- \quad (4)$$

The generated hydroxyl then crosses the anion exchange membrane to accomplish the circuit. This working principle enables the organics to be degraded and the electricity to be generated simultaneously.

3.2 Photoanode characterization

To acquire the crystalline phase and morphology of the prepared photoanode on the carbon paper, a D8 ADVANCE X-ray diffraction (Bruker, Germany) and a S4800 field emission scanning electron microscope (Hitachi, Japan) were characterized. Figure 3 shows the XRD pattern of the pure TiO_2 and CdS-ZnS sensitized TiO_2 samples. As can be seen, for the pure TiO_2, two crystalline phases, i.e. anatase-TiO_2 and rutile-TiO_2, could be observed. Whereas for the CdS-ZnS modified TiO_2, two good crystalline phases of anatase-TiO_2 and rutile-TiO_2 could still be observed, indicating that the structure of TiO_2 can be maintained during the photosensitization process. Besides, it can also be found that several weak peaks corresponding to CdS and ZnS could also be

identified, proving the existence of photosensitizers. Furthermore, to quantitatively characterize the component ratio of the CdS-ZnS sensitizing agents in the prepared photoanode, a 7500ce inductively coupled plasma mass spectrometry (Agilent, USA) was also employed to measure the amount of cadmium and zinc species. The results show that the mass percentage of Cd and Zn species were about 4.54% and 0.78%, respectively. It is indicated that the molar ratio of CdS and ZnS was about 3.39 : 1, which approximated to the ionic concentration ratio of cadmium nitrate and zinc nitrate in the mixed solution.

Figure 4 shows the top-view images of the pure TiO_2 layer and the CdS-ZnS/TiO_2 layer on the carbon paper, respectively. It can be found that the bare TiO_2 film showed vigorous porous structure (see Figure 4a). While for the visible light responsive photoanode, some large clusters consisting of CdS and ZnS nanoparticles with ultra-small size (see the inset of Figure 4b) could also be observed. Figure 5 shows the morphology and element distribution of the CdS-ZnS/TiO_2 photoanode at the cross-sectional view. As can be seen, there existed a distinct layered structure. A thinner layer with the thickness ranging from 0.6 μm to 1 μm was formed on the top of the TiO_2 layer. These results further indicated the presence of the CdS-ZnS photosensitizers in the prepared photoanode. In addition, it can also be found that both the cadmium and zinc signal were also present in the TiO_2 layer (see Figure 5), which signified that the photosensitizers of CdS and ZnS were formed between the titania nanoparticles.

In addition, to verify the visible-light response of the CdS-ZnS photosensitized photoanode, diffuse reflectance UV-Visible absorption spectra was also characterized, and the result is shown in Figure 6. For the bare TiO_2 sample, the main absorption region was in the UV region (< 400 nm). While for the CdS-ZnS sensitized TiO_2 sample, benefited from the comparatively lower band gap of the CdS, the excitation wavelength can be extended [35], resulting in extended absorption spectrum to the visible light region (~ 550 nm). It should be mentioned that only the narrow band gap material of CdS has already been able to respond to the visible light, and then enhance the utilization of solar energy. Once light illuminates the photocatalysts, the photo-excited electrons in CdS are transferred to TiO_2 because of the more positive conduction band of CdS, while the remaining holes in CdS promotes the charge separation [33]. However, CdS also faces a critical problem of severe photo-corrosion, which significantly inhibits its widespread application [36]. Fortunately, the band gap of ZnS used in the present study is large, which can be used to not only passivate CdS to avoid the photo-corrosion but also promote the separation of charge carriers to inhibit the recombination [30]. These results indicated that the CdS-ZnS quantum-dots-sensitization can allow the prepared photoanode to well and stably respond to the visible light.

3.3 Performance evaluation

In this section, to clearly state the membrane effect on the cell performance, the typical polarization curves were measured to characterize the performances of the proton exchange membrane (Nafion® 211) based membrane electrode assembled

photoelectrochemical cell (PMEA-PEC) and the AMEA-PEC. To highlight the membrane effect, the PECs were both fabricated with a CdS-ZnS/TiO_2 photoanode and an air-breathing cathode. Besides, to elaborate the role of CdS-ZnS, the performances of the AMEA-PECs with the CdS-ZnS/TiO_2 and pure TiO_2 photoanodes were also visited. For fair comparison, the other operating conditions were kept the same. Here, the light intensity was set at 180 mW/cm^2, the electrolyte of 0.2 M KOH along with 20% ethanol by volume was used as the simulated wastewater. The liquid flow rate was 100 μL/min. Figure 7a shows the polarization and power density curves of the fabricated PECs. One should note that because the light can only transmit through the channel region of the current collector at the photoanode, the calculations of the current density and power density are based on the effective illumination area, which is half of the MEA area. The results showed that because the pure TiO_2 can only respond to the UV light (see Figure 6), less electron/hole pairs can be photo-excited, leading to poor performance and solar energy utilization efficiency. As a result, the AMEA-PEC with pure TiO_2 photoanode presented the lowest cell performance. Besides, it can also be seen that the AMEA-PEC yielded better performance than did the PMEA-PEC. For the PMEA-PEC, the OCV and SCCD were 1.03 V and 1.50 mA/cm^2, respectively, and the maximum power density was 0.45 mW/cm^2, while the OCV and SCCD were increased to 1.29 V and 2.50 mA/cm^2 with the maximum power density of 0.79 mW/cm^2 for the AMEA-PEC. The main reason for the remarkable intensification in the cell performance could be ascribed to the enhanced hydroxyl transport by the anion exchange membrane. As mentioned above, during the working process, the photo-

excited holes were captured by hydroxyl at the photoanode, forming hydroxyl radicals with strong oxidizability to oxidize ethanol (see Eqs. (2-3)). Theoretically, the consumption of hydroxyl at the photoanode could be compensated by the cathode reaction, which transported through the membrane. For the proton exchange membrane, although it allowed for the transport of hydroxyl, mainly relying on diffusion [29], the transfer ability was poorer than that of anion exchange membrane with intrinsic anion transport property. In addition to the transport of hydroxyl through the membrane, the organics crossover through the proton exchange membrane is more serious than the anion exchange membrane due to its weak inhibition property to organics diffusion [37], especially under high ethanol concentrations. But for the anion exchange membrane, benefited from the intensified OH^- transport from the cathode to the photoanode, the ethanol crossover could be inhibited more efficiently [38-40]. Moreover, the thickness of the anion exchange membrane was larger than that of the proton exchange membrane, which was also beneficial for the reduction in the ethanol crossover. To verify this point, we devised an H-type cell with two chambers separated by an anion exchange membrane or a proton exchange membrane. The solution contained 20% ethanol by volume was put in one chamber and pure water was put into another chamber. We then tested the variation of the ethanol concentration in the initial pure water contained chamber using a gas chromatograph (GC-2010 Plus, Shimadzu, Japan) with time for 5 h. The results are shown in Figure 7b. As seen, the ethanol crossover with the anion exchange membrane was an order lower than the proton exchange membrane. Befitted from the lowered ethanol crossover in association with the employed anion exchange

membrane, the mixed potential at the cathode was lowered, thereby further enhancing the cell performance of the AMEA-PEC [40]. In conclusion, the AMEA-PEC was able to present better performance than did the PMEA-PEC due to intrinsic anion transfer property and lowered ethanol crossover.

3.4 Parametric study

Considering that the photoelectrochemical reaction in the case of feeding the electrolyte and ethanol is driven by the light illumination, both the light intensity and the ethanol concentration as well as the electrolyte concentration could play significant roles in the performance of the designed AMEA-PEC. Hence, the effects of the light intensity, the ethanol concentration as well as the electrolyte concentration on the cell performance were studied in this section. To illustrate the feasibility of the proposed AMEA-PEC, particular attention was paid to the cell performances under various operating conditions like high electrolyte concentration and high ethanol concentration.

3.4.1 Electrolyte concentration

Since the OH^- ions in the solution not only function as the charger carriers through the membrane but also can be used as hole scavengers to prevent the recombination of electro-hole pairs at the photoanode, the exploration of the electrolyte concentration on the cell performance is essential. In this part, the light intensity of 180 mW/cm^2 was chosen to simulate solar illumination, the ethanol concentration and liquid flow rate were kept at 10% by volume and 100 μL/min, respectively. The KOH concentrations

were set at 0.1 M, 0.2 M and 0.3 M. Figure 8 shows the variations of the polarization and power density curves with the KOH concentration. As can be seen in Figure 8a, the OCV of about 1.22 V at low KOH concentration (0.1 M) was slightly smaller than that at high concentrations of about 1.23 V. This is because the increase of the KOH concentration means more OH^- ions to scavenge the holes and thus promotes the separation of the photo-generated electron-hole pairs, enhancing the photoelectrochemical reaction kinetics at the photoanode and resulting in the decrease of the photoanode potential. On the other hand, it can also promote the kinetics of the cathodic oxygen reduction reaction, leading to the increase of the cathode potential [11]. Hence, the OCV at low KOH concentration was lower than that at high KOH concentration. Besides, it can also be found that for all KOH concentrations, because the increase of the current density resulted in the increased overpotentials of both the photoanode and cathode, the cell voltage decreased almost linearly with the increase of the current density. As the KOH concentration increased, the cell performance was increased. The SCCD was gradually intensified from 1.80 mA/cm^2 to 2.50 mA/cm^2. For high electrolyte concentration, more OH^- ions can capture the photo-excited holes and form more hydroxyl radicals, which enhanced the photoelectrochemical reaction rate at the photoanode. On the other hand, although the transport of the generated OH^- ions from the cathode to the photoanode through the membrane was inevitable, the increased OH^- concentration at the photoanode could resist the transfer of the OH^- ion. In this case, to ensure the OH^- ion transport, the OH^- concentration at the cathode might be increased, thus enhancing the cathodic reduction reaction kinetics [41-43]. It should be

pointed out that the inhibited transfer of the OH^- ion from the cathode to the photoanode through the membrane may restrict the photoelectrochemical reactions. But the more KOH feeding to the photoanode during the operation might result in the superfluous OH^- ions at the photoanode. Hence, although the transfer of the OH- ions generated by the cathodic reaction was resisted, excess OH^- ions at the photoanode and the enriched OH^- ions at the cathode can still promote the photoelectrochemical reaction at the photoanode and the electrochemical reaction at the cathode, respectively. Because of the above reasons, high electrolyte concentration exhibited better performance. Correspondingly, as can be seen in Figure 8b, the maximum power density was intensified from 0.61 mW/cm^2 to 0.86 mW/cm^2.

3.4.2 Ethanol concentration

In this part, the cell performances of the AMEA-PEC operated under different ethanol concentrations are discussed. Here, the liquid flow rate, the light intensity and the electrolyte concentration were kept at 180 mW/cm^2, 100 μL/min and 0.2 M, respectively. To verify the proposed cell that is able to be operated with high organics concentration, the ethanol concentration was gradually increased from a critically low concentration of 1% to a high concentration of 20% by volume. Figure 9 shows the variations of the polarization and power density curves. As shown, both the OCV and SCCD as well as the maximum power output were gradually intensified with the increased ethanol concentration. When the ethanol concentration increased from 1% to 20%, the OCV gradually increased from 1.06 V to 1.29 V and the SCCD was increased

from 1.8 mA/cm^2 to 2.5 mA/cm^2 (see Figure 9a). Correspondingly, as shown in Figure 9b, the maximum power density was boosted from 0.55 mW/cm^2 to 0.79 mW/cm^2. This is because low ethanol concentration also indicated the limited mass transport for the photoelectrochemical reaction. Once the ethanol transport was promoted, the discharging performance of the proposed AMEA-PEC could be enhanced. For conventional PMEA-PEC, the ethanol crossover through the proton exchange membrane under high ethanol concentration was rather severe, causing the mixed potential at the cathode to be greatly increased and thus decreasing the cell performance [8]. But for the AMEA-PEC, the performance was always increased in the testing range, demonstrating that the ethanol crossover through the anion exchange membrane used in this work and the mixed potential at the cathode could be weakened. This fact indicates the superiority of the developed AMEA-PEC, particularly at relatively high ethanol concentration operation.

3.4.3 Light intensity

Since the photoelectrochemical reaction at the photoanode is actuated by the light illumination, the light intensity plays a vital role in influencing the cell performance. Hence, in this part, the effect of the light intensity was investigated. Here, the ethanol concentration, the KOH concentration and the liquid flow rate were maintained at 10% by volume, 0.2 M and 100 μL/min, respectively. The light intensity ranged from 100 mW/cm^2 to 180 mW/cm^2. Figures. 10a and 10b show the variations of the polarization and power output curves under different light densities. It can be found that, with

increasing the light density, the cell performance was gradually upgraded. As shown in Figure 10a, the OCV increased from 1.15 V (100 mW/cm^2) to 1.23 V (180 mW/cm^2) and the SCCD increased from 1.70 mA/cm^2 (100 mW/cm^2) to 2.2 mA/cm^2 (180 mW/cm^2). Correspondingly, the maximum power density was gradually increased from 0.55 mW/cm^2 to 0.72 mW/cm^2 (see Figure 10b). This is mainly attributed to the enhanced photoelectrochemical reaction rate at the photoanode. Since the increased light illumination can generate more photo-excited electron-hole pairs, which allowed for more hydroxyl radicals to be generated, the photoanode reaction rate was accelerated and the cell performance was improved. Although the increased light intensity can enhance the power generation, the maximum light utilization efficiency, which was defined as the maximum generated power over by illumination power in this work, was gradually declined (see Figure 10c). This is because the probability of the recombination of the electron-hole pairs was also significantly aggravated despite the increased light intensity could excite more electron-hole pairs. As a result, although the maximum power density was gradually intensified with increasing the light intensity, the maximum light utilization efficiency was gradually lowered.

4 Conclusions

This study highlights an anion exchange membrane based membrane electrode assembled photoelectrochemical cell with a visible light responsive CdS-ZnS/TiO_2 photoanode and an air-breathing cathode for simultaneously degrading organics and generating electricity. Such design can not only make the PEC system more compact

and flexible but also effectively enhance the mass transport. In addition, the anion exchange membrane employed in the PEC also facilitated the OH^- transport and reduced the organics crossover. Due to the above-mentioned advantages, the proposed AMEA-PEC was able to yield better performance than did the PMEA-PEC. Besides, the electricity generation characteristics of the developed AMEA-PEC was also explored under different operating conditions. Experimental results show that, the increase of the electrolyte concentration could yield higher performance because of more efficient hydroxyl radical generation at the photoanode. Besides, it is also found that the cell performance was always improved with the increase of the ethanol concentration in the testing range, which indicated that the ethanol crossover could be inhibited by the use of the anion exchange membrane and thus the mixed potential at the cathode was lowered. With the increased light intensity, the cell performance could also be improved due to more photo-excited electron-hole pairs, but the maximum light utilization efficiency was decreased. The above results demonstrate the feasibility of the use of the anion exchange membrane in the photoelectrochemical cells. In addition, the obtained results also indicate that although the proposed AMEA-PEC can distinctly intensify the performance, the ability of wastewater treatment and electricity output are still relatively small. Integrating numerous PECs may be expected to be a possible approach to solve this issue and meet the requirement of real applications.

Acknowledgments

The authors gratefully acknowledge the financial supports of the National Natural Science Foundation of China (No. 51925601, No. 51620105011 and No. 51776026) and the National High-tech Research and Development Program of China (No. 2015AA043503), the Program for Back-up Talent Development of Chongqing University (No. CQU2017HBRC1A01), the Fundamental Research Funds for the Central Universities (No. 2018CDXYDL0001) and the Research Grants Council of the Hong Kong Special Administrative Region, China (No. 25211817).

References

(1) Dincer, I.; Rosen, M. A., Energy, environmental and sustainable development. *Appl. Energ.* **1999,** 64, 427-440.

(2) Li, L.; Wang, G.; Chen, R.; Zhu, X.; Wang, H.; Liao, Q.; Yu, Y., Optofluidics based micro-photocatalytic fuel cell for efficient wastewater treatment and electricity generation. *Lab Chip* **2014,** 14, 3368-75.

(3) Jacobson, M. Z., Review of solutions to global warming, air pollution, and energy security. *Energ. Environ. Sci.* **2009,** 2, 148-173.

(4) Liu, Y. L.; Wang, R. Z.; Xia, Z. Z., Experimental study on a continuous adsorption water chiller with novel design. *Int. J. Refrig.* **2005,** 28, 218-230.

(5) Camacho, L.; Dumée, L.; Zhang, J.; Li, J.-d.; Duke, M.; Gomez, J.; Gray, S., Advances in membrane distillation for water desalination and purification applications. *Water* **2013,** 5, (1), 94-196.

(6) Comninellis, C.; Kapalka, A.; Malato, S.; Parsons, S. A.; Poulios, I.; Mantzavinos, D., Advanced oxidation processes for water treatment: advances and trends for R&D. *J. Chem. Technol. Biot.* **2008,** 83, 769-776.

(7) Hatzinger, P. B., Perchlorate biodegradation for water treatment. *Environ. Sci. Technol.* **2005,** 39, 239A-247A.

(8) Chen, M.; Chen, R.; Zhu, X.; Liao, Q.; An, L.; Ye, D.; Zhou, Y.; He, X.; Zhang, W., A membrane electrode assembled photoelectrochemical cell with a solar-responsive cadmium sulfide-zinc sulfide-titanium dioxide/mesoporous silica photoanode. *J. Power Sources* **2017,** 371, 96-105.

(9) Wang, D.; Li, Y.; Li Puma, G.; Lianos, P.; Wang, C.; Wang, P., Photoelectrochemical cell for simultaneous electricity generation and heavy metals recovery from wastewater. *J. Hazard. Mater.* **2017,** 323, 681-689.

(10) Li, L.; Xue, S.; Chen, R.; Liao, Q.; Zhu, X.; Wang, Z.; He, X.; Feng, H.; Cheng, X., Performance characteristics of a membraneless solar responsive photocatalytic fuel cell with an air-breathing cathode under different fuels and electrolytes and air conditions. *Electrochim. Acta* **2015,** 182, 280-288.

(11) Liao, Q.; Li, L.; Chen, R.; Zhu, X.; Wang, H.; Ye, D.; Cheng, X.; Zhang, M.; Zhou, Y., Respective electrode potential characteristics of photocatalytic fuel cell with visible-light responsive photoanode and air-breathing cathode. *Int. J. Hydrogen Energ.* **2015,** 40, 16547-16555.

(12) Liu, Y.; Li, J.; Zhou, B.; Lv, S.; Li, X.; Chen, H.; Chen, Q.; Cai, W., Photoelectrocatalytic degradation of refractory organic compounds enhanced by a photocatalytic fuel cell. *Appl. Catal. B: Environ.* **2012,** 111, 485-491.

(13) Liu, Y.; Li, J.; Zhou, B.; Li, X.; Chen, H.; Chen, Q.; Wang, Z.; Li, L.; Wang, J.; Cai, W., Efficient electricity production and simultaneously wastewater treatment via a high-performance photocatalytic fuel cell. *Water Res.* **2011,** 45, 3991-8.

(14) Li, L.; Chen, R.; Zhu, X.; Liao, Q.; Wang, H.; An, L.; Zhang, M., A cascading gradient pore microstructured photoanode with enhanced photoelectrochemical and photocatalytic activities. *J. Catal.* **2016,** 344, 411-419.

(15) Shao, P.; Ren, Z.; Tian, J.; Gao, S.; Luo, X.; Shi, W.; Yan, B.; Li, J.; Cui, F., Silica hydrogel-mediated dissolution-recrystallization strategy for synthesis of ultrathin α-Fe_2O_3 nanosheets with highly exposed (110) facets: A superior photocatalyst for degradation of bisphenol S. *Chem. Eng. J.* **2017,** 323, 64-73.

(16) Shao, P.; Tian, J.; Duan, X.; Yang, Y.; Shi, W.; Luo, X.; Cui, F.; Luo, S.; Wang, S., Cobalt silicate hydroxide nanosheets in hierarchical hollow architecture with maximized cobalt active site for catalytic oxidation. *Chem. Eng. J.* **2019,** 359, 79-87.

(17) Asahi, R.; Morikawa, T.; Ohwaki, T.; Aoki, K.; Taga, Y., Visible-light photocatalysis in nitrogen-doped titanium oxides. *Science* **2001,** 293, 269-71.

(18) Wang, D.; Li, Y.; Li Puma, G.; Wang, C.; Wang, P.; Zhang, W.; Wang, Q., Dye-sensitized photoelectrochemical cell on plasmonic Ag/AgCl @ chiral TiO_2 nanofibers for treatment of urban wastewater effluents, with simultaneous production of hydrogen and electricity. *Appl. Catal. B: Environ.* **2015,** 168, 25-32.

(19) Bousiakou, L. G.; Ivanda, M.; Mikac, L.; Raptis, D.; Gotic, M.; Lianos, P.; Jurschat, K.; Johnston, C., Structural, morphological and Raman studies of CdS/CdSe sensitized TiO_2 nanocrystalline thin films for quantum dot sensitized solar cell applications. *Curr. Nanosci.* **2018,** 14, 421-431.

(20) He, Z.; Li, Y.; Zhang, Q.; Wang, H., Capillary microchannel-based microreactors with highly durable ZnO/TiO_2 nanorod arrays for rapid, high efficiency and continuous-flow photocatalysis. *Appl. Catal. B: Environ.* **2010,** 93, 376-382.

(21) Jiang, Z.; Yang, F.; Luo, N.; Chu, B. T.; Sun, D.; Shi, H.; Xiao, T.; Edwards, P. P., Solvothermal synthesis of N-doped TiO_2 nanotubes for visible-light-responsive photocatalysis. *Chem. Commun.* **2008**, 47, 6372-4.

(22) Antoniadou, M.; Daskalaki, V. M.; Balis, N.; Kondarides, D.; Kordulis, C.; Lianos, P., Photocatalysis and photoelectrocatalysis using (CdS-ZnS)/TiO_2 combined photocatalysts. *Appl. Catal. B Environ.* **2011,** 107, 188-196.

(23) Li, K.; Zhang, H.; Tang, T.; Xu, Y.; Ying, D.; Wang, Y.; Jia, J., Optimization and application of TiO_2/Ti-Pt photo fuel cell (PFC) to effectively generate electricity and degrade organic pollutants simultaneously. *Water Res.* **2014,** 62, 1-10.

(24) Antoniadou, M.; Lianos, P., Production of electricity by photoelectrochemical oxidation of ethanol in a PhotoFuelCell. *Appl. Catal. B: Environ.* **2010,** 99, 307-313.

(25) Antoniadou, M.; Lianos, P., Photoelectrochemical oxidation of organic substances over nanocrystalline titania: Optimization of the photoelectrochemical cell. *Catal. Today* **2009,** 144, 166-171.

(26) Frey, T.; Linardi, M., Effects of membrane electrode assembly preparation on the polymer electrolyte membrane fuel cell performance. *Electrochim. Acta* **2004,** 50, 99-105.

(27) Jeng, K.-T.; Liu, Y.-C.; Leu, Y.-F.; Zeng, Y.-Z.; Chung, J.-C.; Wei, T.-Y., Membrane electrode assembly-based photoelectrochemical cell for hydrogen generation. *Int. J. Hydrogen Energ.* **2010,** 35, 10890-10897.

(28) Ampelli, C.; Passalacqua, R.; Genovese, C.; Perathoner, S.; Centi, G., A novel photo-electrochemical approach for the chemical recycling of carbon dioxide to fuels. *Chem. Eng. Trans.* **2011,** 25, 683-688.

(29) An, L.; Zhao, T. S.; Li, Y.; Wu, Q., Charge carriers in alkaline direct oxidation fuel cells. *Energ. Environ. Sci.* **2012,** 5, 7536.

(30) Aslam, M. M.; Ali, S. M.; Fatehmulla, A.; Farooq, W. A.; Atif, M.; Al-Dhafiri, A. M.; Shar, M. A., Growth and characterization of layer by layer CdS–ZnS QDs on

dandelion like TiO_2 microspheres for QDSSC application. *Mat. Sci. Semicon. Proc.* **2015,** 36, 57-64.

(31) Jiao, X.; Chen, R.; Zhu, X.; Liao, Q.; Ye, D.; Zhang, B.; An, L.; Feng, H.; Zhang, W., A microfluidic all-vanadium photoelectrochemical cell for solar energy storage. *Electrochim. Acta* **2017,** 258, 842-849.

(32) Nicolau, Y. F., Solution deposition of thin solid compound films by a successive ionic-layer adsorption and reaction process. *Appl. Surf. Sci.* **1985,** 22-23, 1061-1074.

(33) Antoniadou, M.; Kondarides, D. I.; Dionysiou, D. D.; Lianos, P., Quantum Dot Sensitized Titania Applicable as Photoanode in Photoactivated Fuel Cells. *J. Phys. Chem. C* **2012,** 116, 16901-16909.

(34) Cheng, X.; Chen, R.; Zhu, X.; Liao, Q.; An, L.; Ye, D.; He, X.; Li, S.; Li, L., An optofluidic planar microreactor for photocatalytic reduction of CO_2 in alkaline environment. *Energ.* **2017,** 120, 276-282.

(35) Zhao, W.; Bai, Z.; Ren, A.; Guo, B.; Wu, C., Sunlight photocatalytic activity of CdS modified TiO2 loaded on activated carbon fibers. *Appl. Surf. Sci.* **2010,** 256, 3493-3498.

(36) So, W.-W.; Kim, K.-J.; Moon, S.-J., Photo-production of hydrogen over the CdS–TiO_2 nano-composite particulate films treated with $TiCl_4$. *Int. J. Hydrogen Energ.* **2004,** 29, 229-234.

(37) Sungpet, A., Reduction of alcohol permeation through Nafion® by polypyrrole. *J. Membrane Sci.* **2003,** 226, 131-134.

(38) Varcoe, J. R.; Slade, R. C., Prospects for alkaline anion-exchange membranes in low temperature fuel cells. *Fuel Cells* **2004,** 5, 187-200.

(39) Zakaria, Z.; Kamarudin, S. K.; Timmiati, S. N., Membranes for direct ethanol fuel cells: An overview. *Appl. Energ.* **2016,** 163, 334-342.

(40) Heinzel, A.; Barragan, V. M., A review of the state-of-the-art of the methanol crossover in direct methanol fuel cells. *J. Power Sources* **1999,** 84, 70-74.

(41) Antolini, E.; Gonzalez, E. R., Alkaline direct alcohol fuel cells. *J. Power Sources* **2010,** 195, 3431-3450.

(42) An, L.; Zhao, T. S.; Shen, S. Y.; Wu, Q. X.; Chen, R., Alkaline direct oxidation fuel

cell with non-platinum catalysts capable of converting glucose to electricity at high power output. *J. Power Sources* **2011,** 196, 186-190.

(43) An, L.; Zhao, T. S.; Chen, R.; Wu, Q. X., A novel direct ethanol fuel cell with high power density. *J. Power Sources* **2011,** 196, 6219-6222.

Figure Captions

Figure 1 Schematic illustrations of (a) the membrane electrode assembled PEC and (b) the experimental system.

Figure 2 Schematic illustration of the working principle of the anion exchange membrane based membrane electrode assembled PEC.

Figure 3 XRD patterns of the TiO_2 before and after photosensitization.

Figure 4 FESEM images of (a) the TiO_2 film and (b) the CdS-ZnS/TiO_2 film on the carbon paper.

Figure 5 FESEM morphology and element distribution of the CdS-ZnS/TiO_2 photoanode at the cross-sectional view.

Figure 6 UV-Vis adsorption spectra of the TiO_2 and CdS-ZnS/TiO_2.

Figure 7 (a) Typical polarization and power density curves of the fabricated PECs (Light intensity: 180 mW/cm^2, KOH concentration: 0.2 M, ethanol concentration: 20% by volume, liquid flow rate: 100 μL/min) and (b) Variation of the ethanol concentration in the initial pure water contained chamber with time (Ethanol concentration in the initial ethanol contained chamber: 20% by volume).

Figure 8 Effect of the KOH concentration the (a) polarization curve and (b) power density curve. (Light intensity: 180 mW/cm^2, ethanol concentration: 10% by volume, liquid flow rate: 100 μL/min)

Figure 9 Effect of the ethanol concentration on the (a) polarization curve and (b) power density curve. (Light intensity: 180 mW/cm^2, KOH concentration: 0.2 M, liquid flow rate: 100 μL/min)

Figure 10 Effect of the light intensity on (a) the polarization and (b) power density curves, and (c) Variation of the light utilization efficiency with the light intensity. (KOH concentration: 0.2 M, ethanol concentration: 10% by volume, liquid flow rate: 100 μL/min)

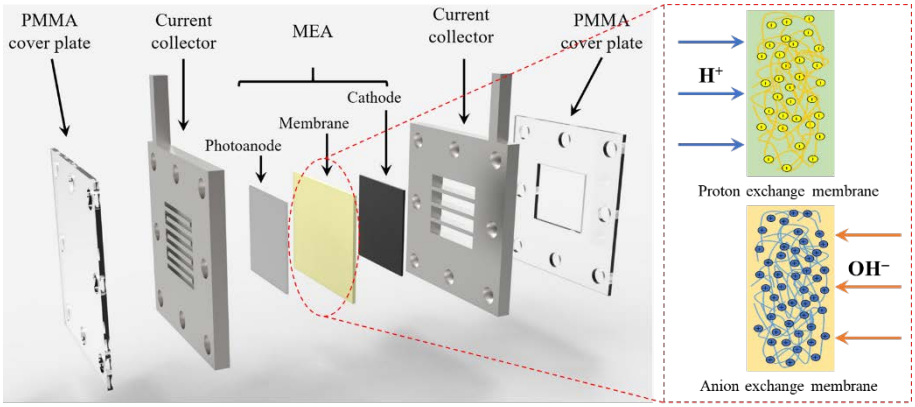

(a)

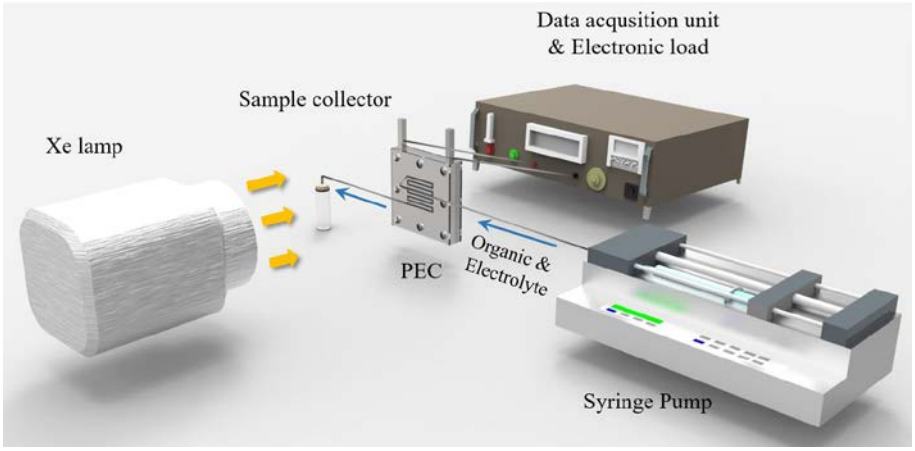

(b)

Figure 1 Schematic illustrations of (a) the membrane electrode assembled PEC and (b) the experimental system.

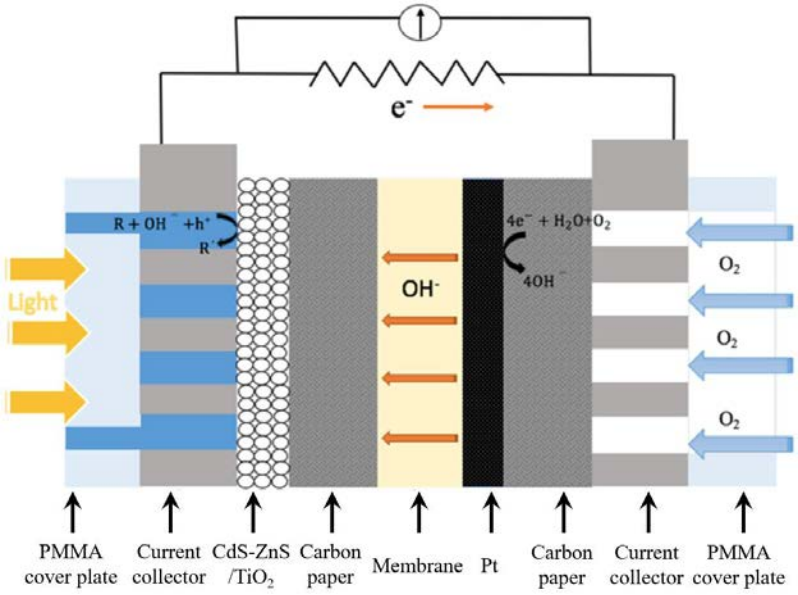

Figure 2 Schematic illustration of the working principle of the anion exchange membrane based membrane electrode assembled PEC

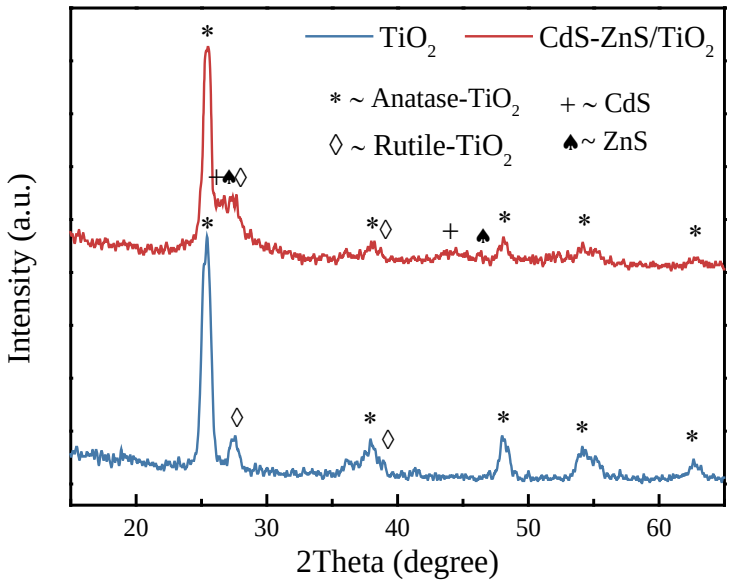

Figure 3 XRD patterns of the TiO_2 before and after photosensitization.

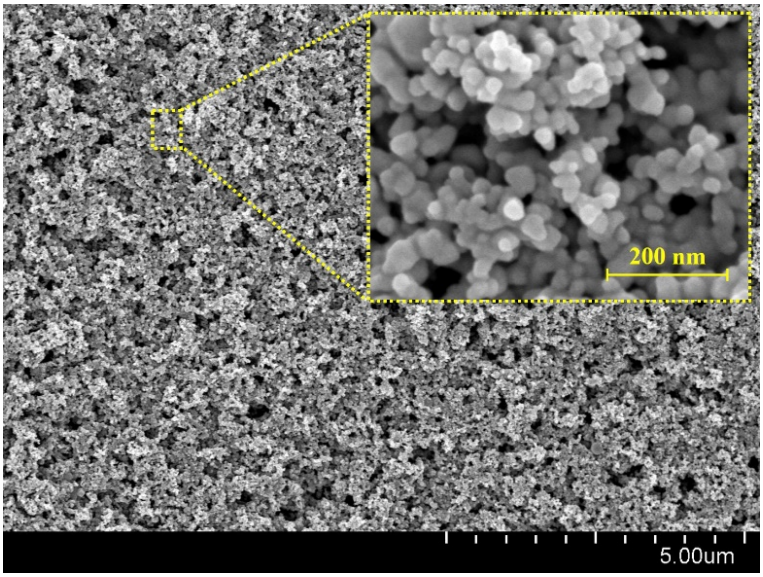

(a)

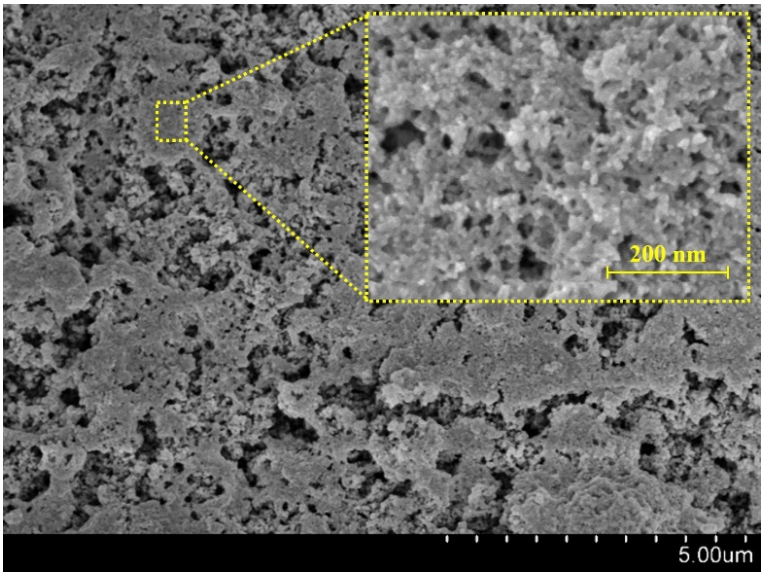

(b)

Figure 4 FESEM images of (a) the TiO_2 film and (b) the CdS-ZnS/TiO_2 film on the carbon paper.

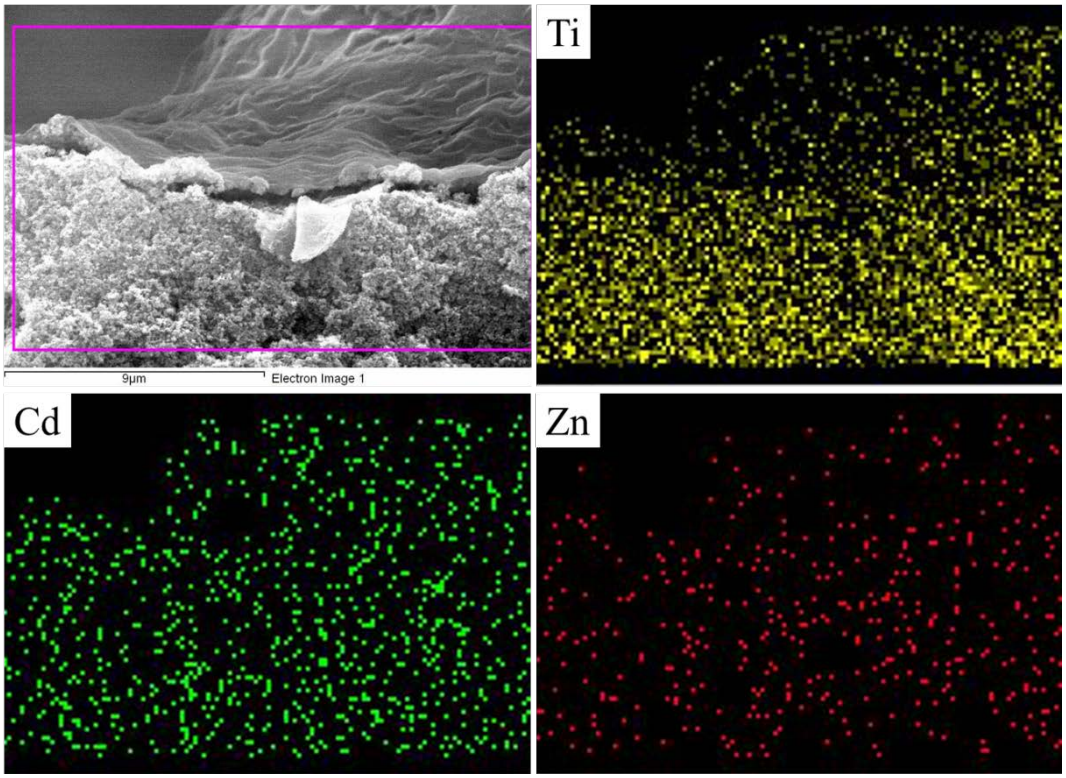

Figure 5 FESEM morphology and element distribution of the CdS-ZnS/TiO_2 photoanode at the cross-sectional view.

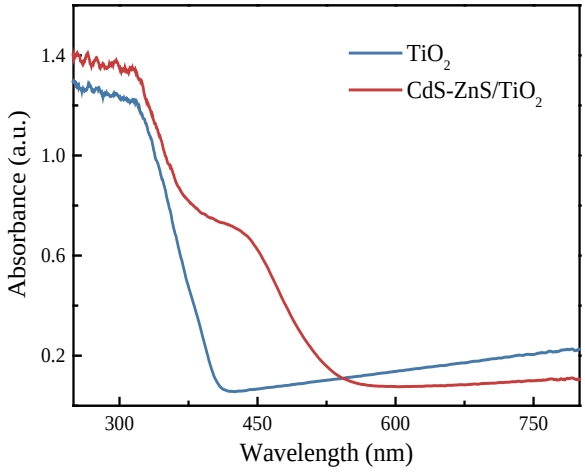

Figure 6 UV-Vis adsorption spectra of the TiO_2 and CdS-ZnS/TiO_2.

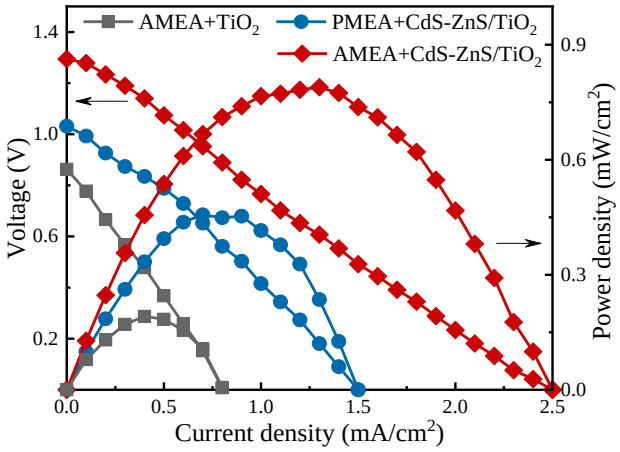

(a)

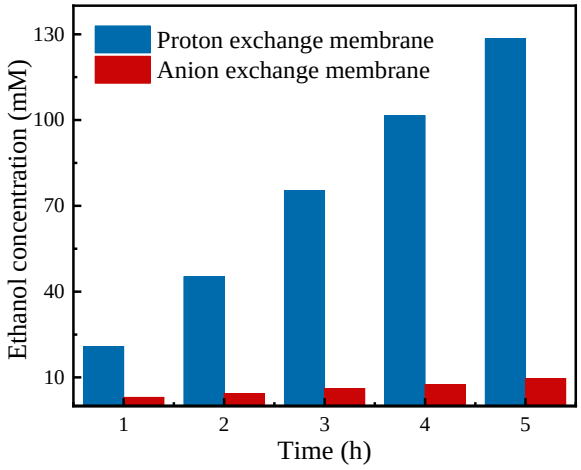

(b)

Figure 7 (a) Typical polarization and power density curves of the fabricated PECs (Light intensity: 180 mW/cm^2, KOH concentration: 0.2 M, ethanol concentration: 20% by volume, liquid flow rate: 100 µL/min) and (b) Variation of ethanol concentration in the initial pure water contained chamber with time (Ethanol concentration in the initial ethanol contained chamber: 20% by volume).

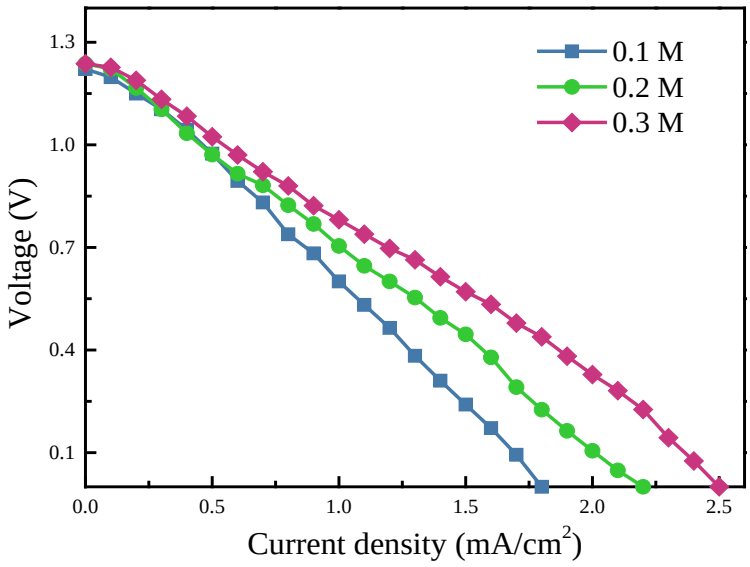

(a)

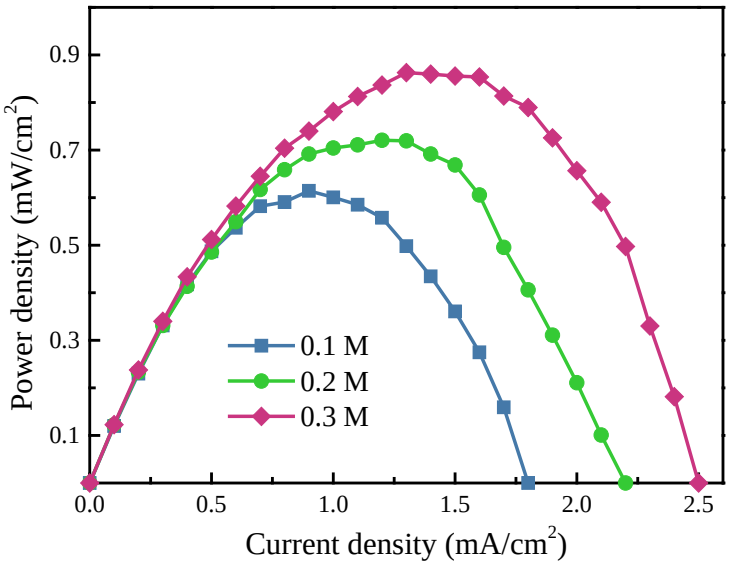

(b)

Figure 8 Effect of the KOH concentration on the (a) polarization curve and (b) power density curve. (Light intensity: 180 mW/cm^2, ethanol concentration: 10% by volume, liquid flow rate: 100 μL/min)

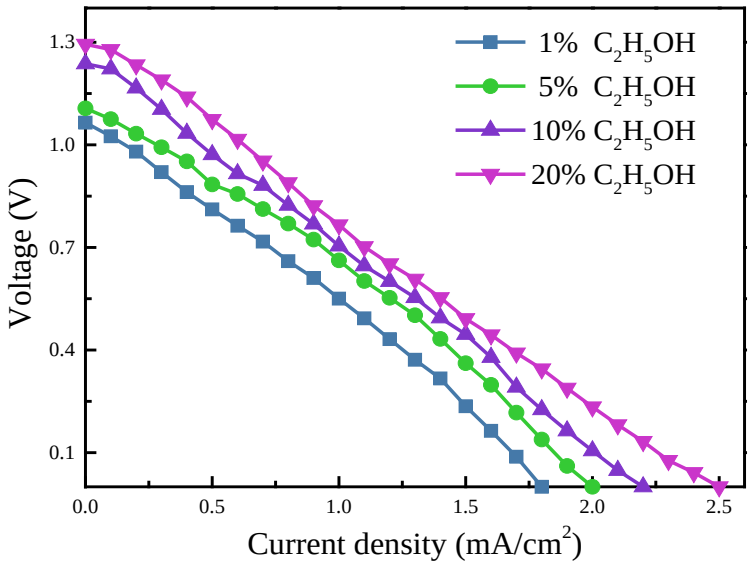

(a)

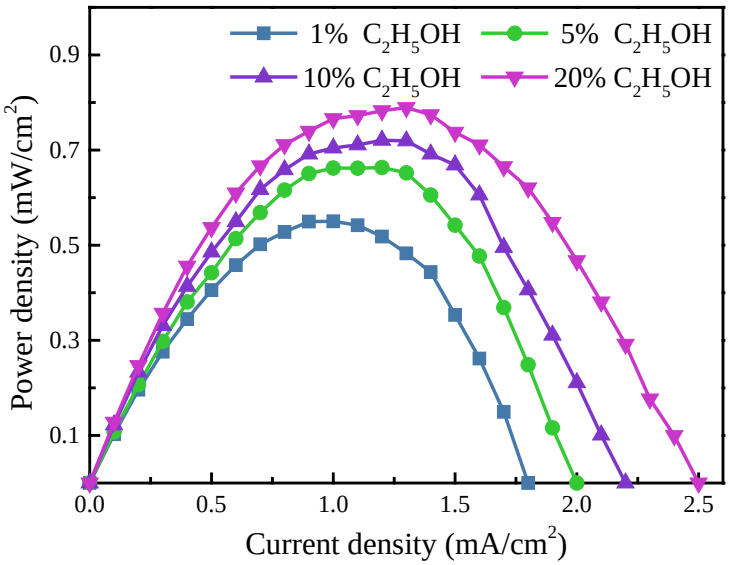

(b)

Figure 9 Effect of the ethanol concentration on the (a) polarization curve and (b) power density curve. (Light intensity: 180 mW/cm^2, KOH concentration: 0.2 M, liquid flow rate: 100 μL/min)

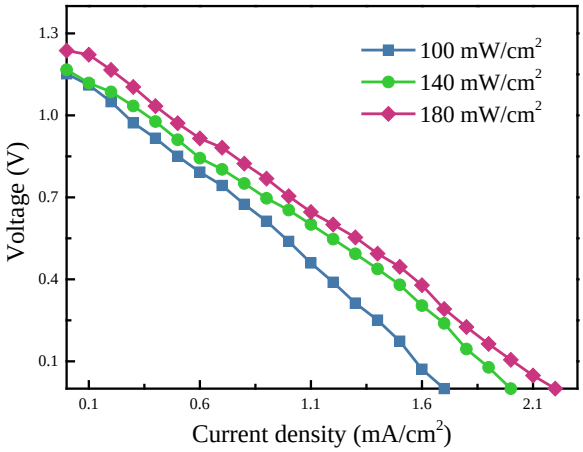

(a)

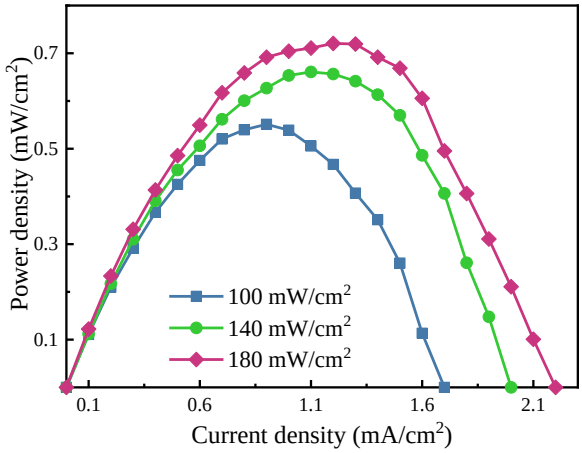

(b)

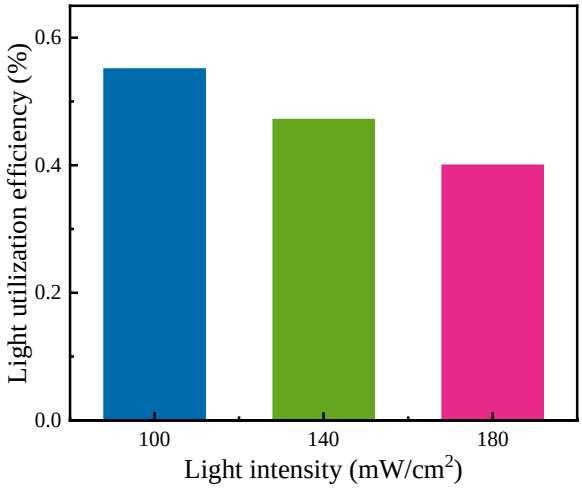

(c)

Figure 10 Effect of the light intensity on (a) the polarization and (b) power density curves, and (c) Variation of the light utilization efficiency with the light intensity. (KOH concentration: 0.2 M, ethanol concentration: 10% by volume, liquid flow rate: 100 μL/min)

For Table of Contents Only